Magn Reson Med Sci 2024; 23; 161–170
doi:10.2463/mrms.mp.2022-0091 Published Online: March 1, 2023

MAJOR PAPER

Application of Texture and Volume Model Analysis to Dedicated Axillary High-resolution 3D T2-weighted MR Imaging: A Novel Method for Diagnosing Lymph Node Metastasis in Patients with Clinically Node-negative Breast Cancer

Hiroaki Shimizu[1,2], Naoko Mori[1*], Shunji Mugikura[1,3], Yui Maekawa[1], Minoru Miyashita[4], Tatsuo Nagasaka[5], Satoko Sato[6], and Kei Takase[1]

Purpose: To evaluate the effectiveness of the texture analysis of axillary high-resolution 3D T2-weighted imaging (T2WI) in distinguishing positive and negative lymph node (LN) metastasis in patients with clinically node-negative breast cancer.

Methods: Between December 2017 and May 2021, 242 consecutive patients underwent high-resolution 3D T2WI and were classified into the training (n = 160) and validation cohorts (n = 82). We performed manual 3D segmentation of all visible LNs in axillary level I to extract the texture features. As the additional parameters, the number of the LNs and the total volume of all LNs for each case were calculated. The least absolute shrinkage and selection operator algorithm and Random Forest were used to construct the models. We constructed the texture model using the features from the LN with the largest least axis length in the training cohort. Furthermore, we constructed the 3 models combining the selected texture features of the LN with the largest least axis length, the number of LNs, and the total volume of all LNs: texture-number model, texture-volume model, and texture-number-volume model. As a conventional method, we manually measured the largest cortical diameter. Moreover, we performed the receiver operating curve analysis in the validation cohort and compared area under the curves (AUCs) of the models.

Results: The AUCs of the texture model, texture-number model, texture-volume model, texture-number-volume model, and conventional method in the validation cohort were 0.7677, 0.7403, 0.8129, 0.7448, and 0.6851, respectively. The AUC of the texture-volume model was higher than those of other models and conventional method. The sensitivity, specificity, positive predictive value, and negative predictive value of the texture-volume model were 90%, 69%, 49%, and 96%, respectively.

Conclusion: The texture-volume model of high-resolution 3D T2WI effectively distinguished positive and negative LN metastasis for patients with clinically node-negative breast cancer.

Keywords: *breast neoplasms, lymph nodes, lymphatic metastasis, magnetic resonance imaging, metastasis*

Introduction

The diagnosis of lymph node (LN) metastasis in patients with breast cancer plays an important role in predicting its prognosis and in determining the treatment strategy. LN metastasis is strongly correlated with overall and disease-free survival.[1–4] Neoadjuvant chemotherapy may be indicated as one form of

[1]Department of Diagnostic Radiology, Tohoku University Graduate School of Medicine, Sendai, Miyagi, Japan
[2]Tohoku University School of Medicine, Sendai, Miyagi, Japan
[3]Division of Image Statistics, Tohoku Medical Megabank Organization, Tohoku University, Sendai, Miyagi, Japan
[4]Department of Surgical Oncology, Tohoku University Graduate School of Medicine, Sendai, Miyagi, Japan
[5]Department of Radiological Technology, Tohoku University Graduate School of Medicine, Sendai, Miyagi, Japan
[6]Department of Anatomic Pathology, Tohoku University Graduate School of Medicine, Sendai, Miyagi, Japan

*Corresponding author: Department of Radiology, Akita University Graduate School of Medicine, 1-1-1, Hondo, Akita, Akita 010-8543, Japan. Phone: +81-22-717-7312, Fax: +81-22-717-7316, E-mail: naokomori7127@gmail.com

Received: August 4, 2022 | Accepted: January 23, 2023

treatment following the preoperative diagnosis of LN metastasis.[5,6]

In clinical practice, MRI is used to evaluate primary breast cancer and axillary LN metastasis.[7,8] Advanced LN metastasis could be detected using morphological changes including shape and diameter on 2D T2 weighted imaging (T2WI); however, for early LN metastasis, the diagnostic performance of 2D T2WI is limited.[9–12] In early LN metastasis, small histological metastatic nests grow within the LNs,[13,14] and it is difficult to detect the condition on 2D T2WI. Schipper et al. reported that 3D T2WI displays high specificity in distinguishing positive and negative LN metastasis by morphological changes.[15] They used a surface coil to image the axillary region. Samiei et al. used bilateral breast coils focusing on the FOV of the axillary region and reported on comparable diagnostic performance to that of a surface coil.[16] Taken together, 3D T2WI with high spatial resolution using bilateral breast coils can detect morphological changes in LN metastasis.[17]

The heterogeneous signal intensity in LNs on T2WI is associated with LN metastasis.[12,18,19] To quantify the morphological changes and heterogeneity of signal intensity in LNs, texture analysis measuring spatial variations could be applied to 3D T2WI. Haralick et al. proposed the grey-level co-occurrence matrix (GLCM) method, one of the texture analysis procedures, which evaluates the arrangement and interrelation among grey-level voxel intensities.[20] Previous studies in uterine reported on the effectiveness of texture analysis on 2D T2WI in distinguishing positive and negative LN metastasis.[21] Moreover, the texture analysis was applied to LNs on 3D T2WI in distinguishing positive and negative LN metastasis in patients with breast cancer by Samiei et al. They included patients with clinically node-negative and node-positive breast cancer.[22] We hypothesized that the texture analysis of high-resolution 3D T2WI could quantitatively evaluate the morphological changes, including the shape and volume, and signal changes caused by metastasis within the LNs.

In this study, we focused on patients with clinically node-negative breast cancer and aimed to evaluate the efficacy of texture analysis of axillary high-resolution 3D T2WI in distinguishing positive and negative LN metastasis.

Materials and Methods

Patients

Our Institutional Review Board approved this retrospective study and waived the requirement for informed consent. Between December 2017 and May 2021, 426 consecutive patients underwent preoperative MRI, including 3D T2WI, followed by mastectomy or lumpectomy. The inclusion criteria were as follows: (a) diagnosis of invasive breast cancer by preoperative biopsy, (b) clinical node-negative breast cancer judged by the breast surgeon to be comprehensively negative for LN metastasis (neither apparently swollen LNs nor irregular thickening of the cortex on MRI or ultrasound), and (c) surgery with sentinel LN biopsy. The exclusion criteria were as follows: (a) neoadjuvant treatment, which might affect the histology of LNs (n = 154) and (b) poor image quality of 3D T2WI (n = 30): cases with strong wrap-around artefacts (n = 18) and those with severe noises because of smaller FOV and larger matrix size (n = 12). In case of bilateral breast cancer (n = 4), we selected the side with larger-sized primary breast cancer. Thus, a total of 242 patients were included in this study and chronologically separated into two independent cohorts. The training and validation cohorts included 160 and 82 patients between July 2019 and May 2021 and December 2017 and July 2019, respectively. All patients were women with a median age of 55 years (range, 26–87 years).

MR imaging protocol

MR examinations were performed before surgery using a 3.0T MRI unit (Intera Achieva dStream; Philips Healthcare, Best, the Netherlands), with multiple-source radiofrequency transmission for all scans. All patients were imaged in the prone position with both breasts placed in 16-channel bilateral breast coils, and dynamic contrast-enhanced MRI (DCE-MRI) and axillary high-resolution 3D T2WI were performed using the same bilateral breast coils. The DCE-MRI protocol comprised a 3D fat-suppressed T1-weighted gradient-echo sequence (TR/TE, 5.2/2.6 ms; flip angle, 10°; acquisition section thickness, 1.8 mm; FOV, 350 mm; matrix size, 480 × 282, resulting in an in-plane resolution of 0.73 × 1.24 mm^2; and acquisition time, 60s) with an intravenous infusion of 0.1 mmol/kg Gadobutrol (Gadovist; Bayer Yakuhin, Osaka, Japan), followed by 20 mL of saline flush at 2 mL/sec. The high-resolution 3D T2WI protocol was performed centering around the axillary level I region with a FOV of 100 mm. It comprised an axial 3D T2-weighted turbo spin-echo sequence without fat suppression (TR/TE, 2000/210 ms; flip angle, 90°; echo train length, 120; number of signals acquired, one; acquisition section thickness, 1.47 mm; FOV, 100 mm; matrix size, 166 × 166, resulting in an in-plane resolution of 0.6 × 0.6 mm^2; and acquisition time, 5 min 10s).

Image analysis

Manual measurement of the cortical diameter

The MRI Digital Imaging and Communications in Medicine (DICOM) data of 242 patients were displayed on a commercially available workstation (HMC Viewer Ver. V1.0.0; Hitachi, Tokyo, Japan). Two observers (14 and 5 years of experience in breast imaging) independently interpreted the high-resolution 3D T2W images blinded to the patients' clinical information, other imaging findings, and pathological results. They reviewed the data in the axial plane of high-resolution 3D T2W images to visually select the LNs with the largest cortical diameter in the axillary level I region.[23] Subsequently, they manually measured the largest cortical diameter of the LN (Fig. 1a).

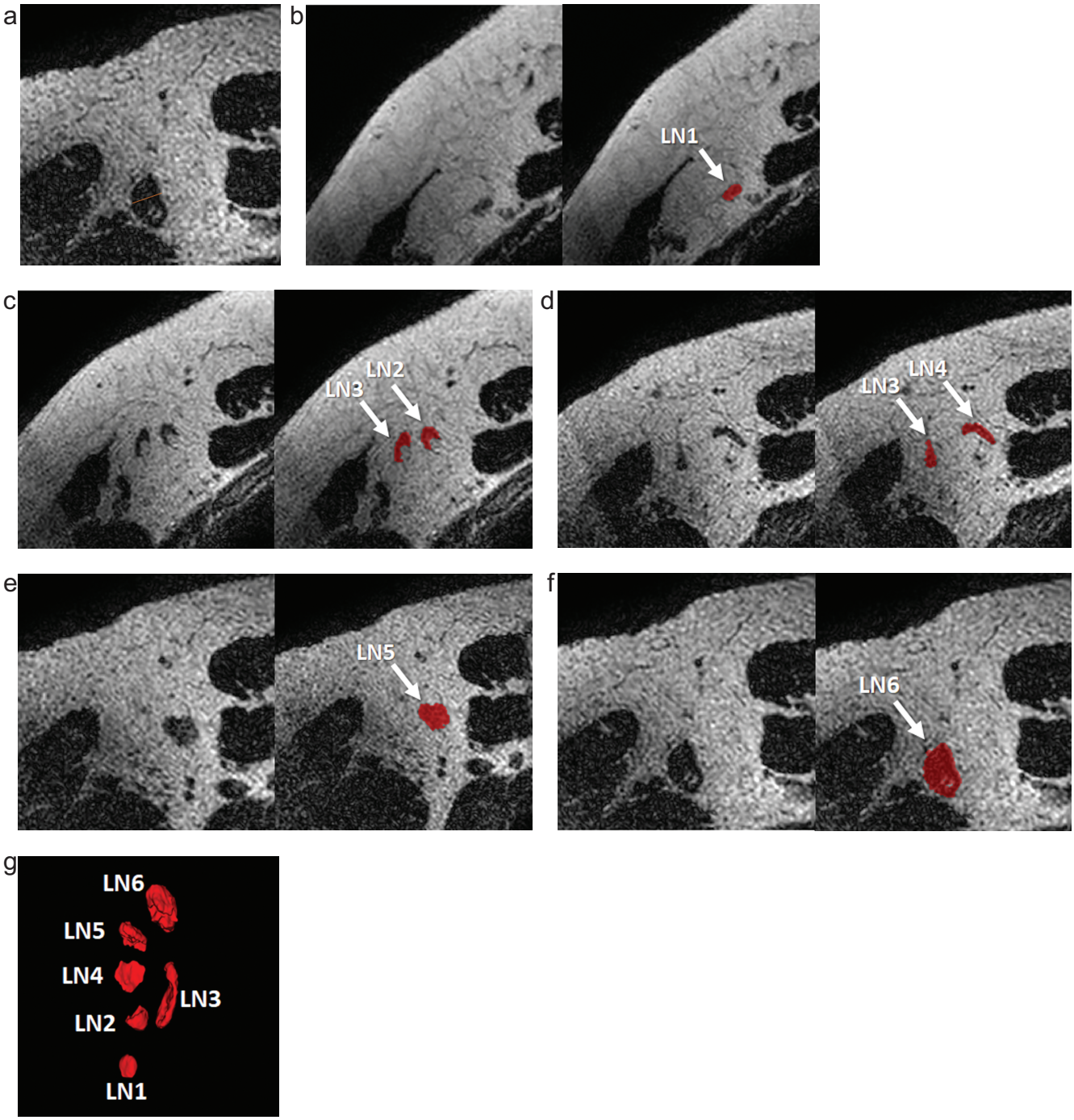

Fig. 1 Manual measurement of the cortical diameter and segmentation of all visible LNs in axillary level I. A 49-year-old woman diagnosed with invasive ductal carcinoma underwent preoperative MRI, including high-resolution 3D T2-weighted imaging. The LN with the largest cortical diameter was selected to manually measure the cortical diameter (**a**). Manual 3D segmentation of all visible LNs in axillary level I was performed using ITK-SNAP (**b–f**), and the 3D volumes of interest for all visible LNs were obtained to extract the texture features. Six LNs were identified on 3D rendering from the coronal view (**g**). In this case, the manual measurement of cortical diameter was 6.41 mm. The volume of all LNs was 1359 mm^3, and the texture-volume model indicated positive LN metastasis. The case was diagnosed as sentinel LN metastasis with a 1.5 mm metastatic nest by sentinel LN biopsy. LN, lymph node.

Segmentation and extraction of the texture features

The MRI DICOM data of 242 patients were transferred to a personal computer. One observer (14 years of experience in breast imaging) performed the semi-automatic 3D segmentation of all visible LNs in axillary level I using an online free software ITK-SNAP (v.3.8.0; www.itksnap.org) on

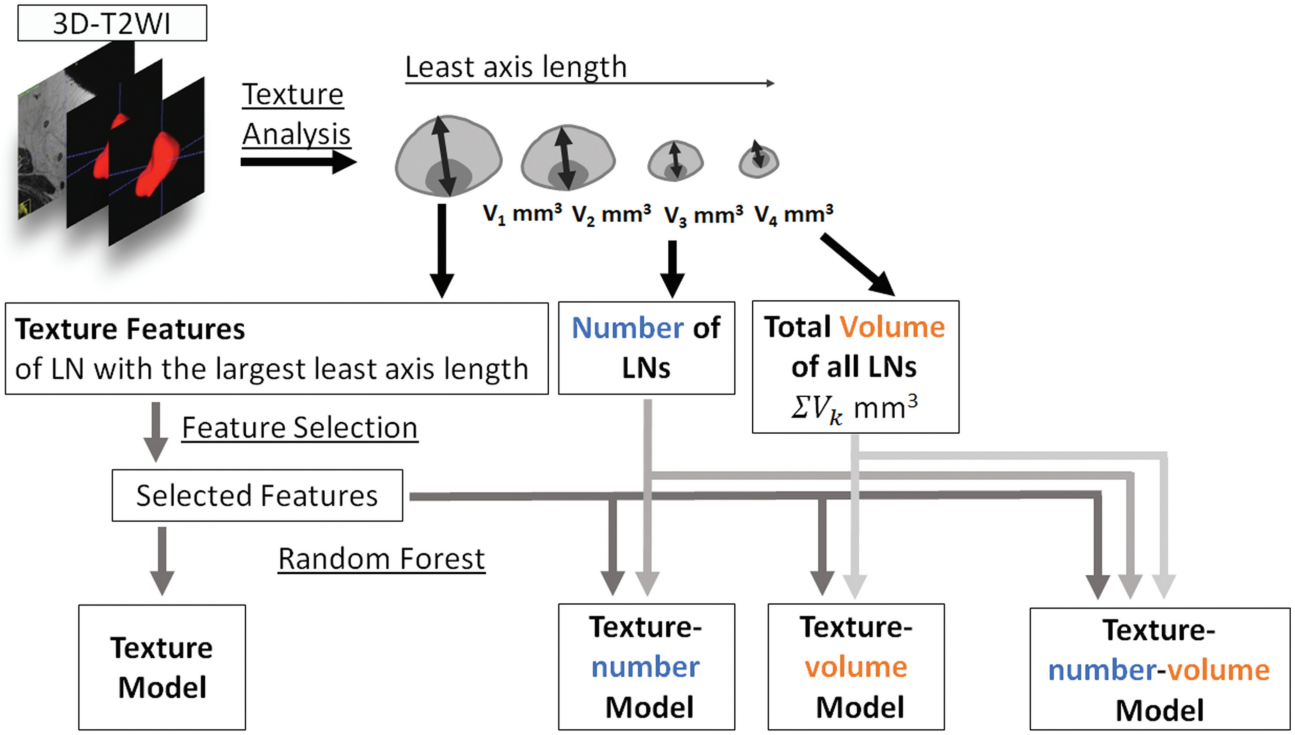

Fig. 2 Flowchart of the texture and texture-model construction. Texture analysis is performed for each LN segmented on 3D T2-weighted images. Feature selection is performed for the texture features of the LN with the largest least axis length. The number of the LNs and the total volume of all LNs defined as the sum of the volumes of all LNs are calculated. The texture model is constructed using the selected texture features of the LN with the largest least axis length by Random Forest. The texture-number model is constructed using the texture features and the number of LNs. The texture-volume model is constructed using the selected texture features of the LN with the largest least axis length and the total volume of all LNs by Random Forest. The texture-number-volume model is constructed using the texture features, the number of LNs, and the total volume of all LNs. LN, lymph node; T2 weighted imaging (T2WI).

high-resolution 3D T2W images (Fig. 1b–1g). The observer was blinded to the patients' clinical information, other imaging findings, and pathological results. We obtained the 3D volumes of interest (VOIs) for all visible LNs in axillary level I to extract the texture features. Texture analysis was performed using the PyRadiomics software (v3.0.1; https://www.pypi.org/project/pyradiomics/). Normalization of signal intensity was performed as pre-processing in the Pyradiomics pipeline. PyRadiomics extracted 90 texture features from the high-resolution 3D T2W images for each LN, including the shape and volume (Supplementary Table 1). The least axis length was calculated as one of the features of PyRadiomics. As the additional parameters, the number of the LNs and the total volume of all LNs for each case were calculated. The total volume of all LNs was calculated as the sum of the volumes of all LNs in axillary level I.

Model construction

Since the number of all visible LNs varied from case to case and texture features are calculated from each LN, it is problematic to determine which LN should be used for model construction. In this study, we hypothesized that the largest LN in a certain case would have the most specific features of the LN in that case. The least axis length of LNs was used to select the LNs as follows. The least axis length of LNs denotes the smallest axis length of the ellipsoid enclosing the VOI and was obtained as one of texture features. It was considered similar to the largest cortical diameter of the LN, and the LNs with the largest least axis length was selected as the representative LN in each case (Fig. 2). The LN with the largest least axis length was not identical to the LN assessed in the manual measurement of the cortical diameter. For the texture features of the LN with the largest least axis length, we performed feature selection by the least absolute shrinkage and selection operator (LASSO) algorithm.[21,24–26] We constructed the texture model using the selected texture features of the LN with the largest least axis length by Random Forest (Fig. 2). Furthermore, we constructed the 3 models combining the selected texture features of the LN with the largest least axis length, the number of LNs, and the total volume of all LNs using Random Forest. The texture-number model was constructed using the texture features and the number of LNs. The texture-volume model was constructed using the texture feature and the total volume of all LNs. The texture-number-volume model was constructed using the texture features, the number of LNs, and the total

volume of all LNs. In this study, the number of estimators was set at 100 and the maximum depth at 2000.

Statistical analysis

We performed Mann–Whitney U tests to compare the age, diameter of breast cancer, and Ki-67 labelling index between the training and validation cohorts. Fisher's exact tests were conducted to compare the histological type of breast cancer, receptor status of breast cancer, Nottingham's histologic grade, and pathological diagnosis of LN metastasis between the training and validation cohorts. We assessed the inter-observer reliability of the manual measurement of the cortical diameter using the interclass correlation coefficient (ICC) (r = 1.0, perfect agreement; 0.81–0.99, almost perfect agreement; 0.61–0.80, substantial agreement; 0.41–0.60, moderate agreement; 0.21–0.40, fair agreement; and ≤ 0.20, slight agreement).[27] The manual measurement of the cortical diameter by one of the two observers was used for the statistical analysis. Furthermore, in the training and validation cohorts, Mann–Whitney U tests were performed to compare the manual measurement of the cortical diameter, the number of LNs, and the total volume of all LNs between the positive and negative LN metastasis groups. We evaluated the diagnostic performance of the models constructed on the training cohort in differentiating between the positive and negative LN metastasis groups by receiver operating characteristic (ROC) curve analysis. The area under the curves (AUCs) were calculated for the training and validation cohorts. AUCs of the texture model, texture-number model, texture-volume model, texture-number-volume model, and manual measurement of the cortical diameter were compared in the validation cohort. We determined the sensitivity, specificity, positive predictive value (PPV), and negative predictive value (NPV) of the model with the highest AUC in the validation cohort at a cut-off point that maximized the value of the Youden index. Statistical analyses including LASSO and Random Forest were performed using JMP Pro 16 (SAS Institute, Cary, NC, USA). ICC was calculated using SPSS Version 21 (IBM, Armonk, NY, USA). A P-value < 0.05 was considered statistically significant.

Results

We observed a significant difference in the patient age between the training and validation cohorts ($P = 0.0080$) (Table 1). There were no statistically significant differences between the training and validation cohorts in terms of other background factors. Thirty-two of 160 cases and 20 of 82 cases were pathologically diagnosed as positive LN metastasis in the training and validation cohorts, respectively. The isolated tumor cell (ITC) in LN was observed in the validation cohort (n = 1), which was classified as negative LN metastasis. Three out of 32 positive LN metastases in the training cohort and two out of 20 positive LN metastases in the validation cohort were micrometastases with metastases less than 2 mm in size.

In the training cohort, there was no significant difference in the manual measurement of the cortical diameter between the positive and negative LN metastasis groups ($P = 0.1811$) (Table 2). In evaluating the agreement between readers, the ICC for the manual measurement of the cortical diameter was 0.964, thus indicating almost perfect agreement. We identified significant differences in the number of LNs and the total volume of all LNs between the positive and negative LN metastasis groups in the training cohort ($P = 0.0417$ and 0.0027, respectively) (Table 3). During feature selection using the LASSO algorithm, we selected six features with non-zero coefficients for LNs with the largest least axis length as follows: shape least axis length, shape surface volume ratio, GLCM inverse variance, GLCM joint average, GLCM maximal correlation coefficient (MCC), and Gray Level Dependence Matrix (GLDM) large dependence high gray level emphasis (Supplementary Table 1). The AUCs of the texture model, texture-number model, texture-volume model, texture-number-volume model, and manual measurement of the cortical diameter in the training cohort were 0.9944, 0.9963, 0.9949, 0.9832, and 0.5765, respectively (Table 4, Fig. 3).

The validation cohort displayed a significant difference in the manual measurement of the cortical diameter between the positive and negative LN metastasis groups ($P = 0.0132$) (Table 2). While evaluating the agreement between readers, the ICC for the manual measurement of the cortical diameter was 0.960, thereby indicating almost perfect agreement. No significant difference was found between the positive and negative LN metastasis groups in the number of LNs ($P = 0.7439$), while we observed a significant difference in the total volume of all LNs between the two groups ($P = 0.0028$) (Table 3). The AUCs of the texture model, texture-number model, texture-volume model, texture-number-volume model, and manual measurement of the cortical diameter in the validationing cohort were 0.7677, 0.7403, 0.8129, 0.7448, and 0.6851, respectively (Table 4, Fig. 3). The texture-volume model had the highest AUC with sensitivity, specificity, PPV, and NPV; 90%, 69%, 49%, and 96%, respectively.

Discussion

The texture-volume model combining texture features from the LN with the largest least axis length and the total volume of all LNs displayed the highest diagnostic performance in distinguishing positive and negative LN metastasis groups in patients with clinically node-negative breast cancer. We demonstrated the generalization ability of the aforementioned model by classifying the patients into the training and validation cohorts. The model displayed higher diagnostic performance than other models or manual measurement of the cortical diameter.

Table 1 Comparison of patient and lesion characteristics between the training and validation cohorts

Variables	Training cohort (n = 160)	Validation cohort (n = 82)	*P*-value
Age (years)	56 ± 14	60 ± 13	0.0080*
Diameter of breast cancer (mm)	15.9 ± 10.5	18.9 ± 14.9	0.1777
Histological types of breast cancer (n (%))			0.2985
No specific type	137 (85.6)	74 (90.2)	
Invasive lobular carcinoma	10 (6.3)	4 (4.9)	
Mucinous carcinoma	12 (7.5)	2 (2.4)	
Apocrine carcinoma	1 (0.6)	1 (1.2)	
Microinvasive carcinoma	0 (0)	1 (1.2)	
Receptor status of breast cancer (n (%))			
ER positive	147 (92)	72 (88)	0.3560
negative	13 (8)	10 (12)	
PR positive	129 (81)	66 (80)	1.0000
negative	31 (19)	16 (20)	
HER2 positive	15 (9)	12 (15)	0.2804
negative	145 (85)	70 (85)	
Ki-67 labelling index	19.4 ± 16.3	17.6 ± 13.6	0.4468
Nottingham's histologic grade (n (%))			1.0000
1	64 (44)	33 (40)	
2	85 (53)	44 (54)	
3	11 (7)	5 (6)	
Pathological diagnosis of LN metastasis (n (%))			0.5086
Positive	32 (20)	20 (24)	
Negative	128 (80)	62 (76)	

Data are expressed as mean ± standard deviation. *indicates statistical significance. ER, oestrogen receptor; HER2, human epidermal growth factor 2; LN, lymph node; PR, progesterone receptor.

Table 2 Manual measurement of the cortical diameter between the positive and negative LN metastasis groups

Variables	Positive LN metastasis	Negative LN metastasis	*P*-value
Manual measurement of cortical diameter			
Training cohort (mm)	4.320 ± 1.298	4.021 ± 1.435	0.1811
Validation cohort (mm)	4.667 ± 1.236	3.820 ± 1.191	0.0132*

Data are expressed as mean ± standard deviation. *indicates statistical significance. LN, lymph node.

T2WI can effectively distinguish axillary LN metastasis in patients with breast cancer.[7,9,10,12,15,16,28,29] The majority of studies simultaneously imaged the breast and axilla in the large FOV using bilateral breast coils, whereas some studies focused on the axillary region using a surface coil.[7,10] Samiei et al. reported that 3D T2WI focused on the axillary region using bilateral breast coils displayed comparable diagnostic performance as 3D T2WI using a surface coil in the visual

Table 3 Number of LNs and total volume of all LNs between the positive and negative LN metastasis groups

Variables	Positive LN metastasis	Negative LN metastasis	*P*-value
Number of LNs			
Training cohort	5.5 ± 2.8	6.4 ± 2.5	0.0417*
Validation cohort	4.8 ± 2.6	4.5 ± 2.4	0.7439
Total volume of all LNs			
Training cohort (mm^3)	1246 ± 618	1108 ± 528	0.0027*
Validation cohort (mm^3)	945 ± 817	706 ± 528	0.0028*

Data are expressed as mean ± standard deviation. *indicates statistical significance. LN, lymph node.

Table 4 Diagnostic performance of the texture model, texture-volume-number model, texture-volume model, texture-number model, and manual measurement of the cortical diameter for the training and validation cohorts in differentiating between positive and negative LN metastasis groups

Models	AUC in the training cohort	AUC in the validation cohort
Texture model	0.9944	0.7677
Texture-number model	0.9963	0.7403
Texture-volume model	0.9949	0.8129
Texture-volume-number model	0.9832	0.7448
Manual measurement of cortical diameter	0.5765	0.6851

AUC, area under the curve; LN, lymph node.

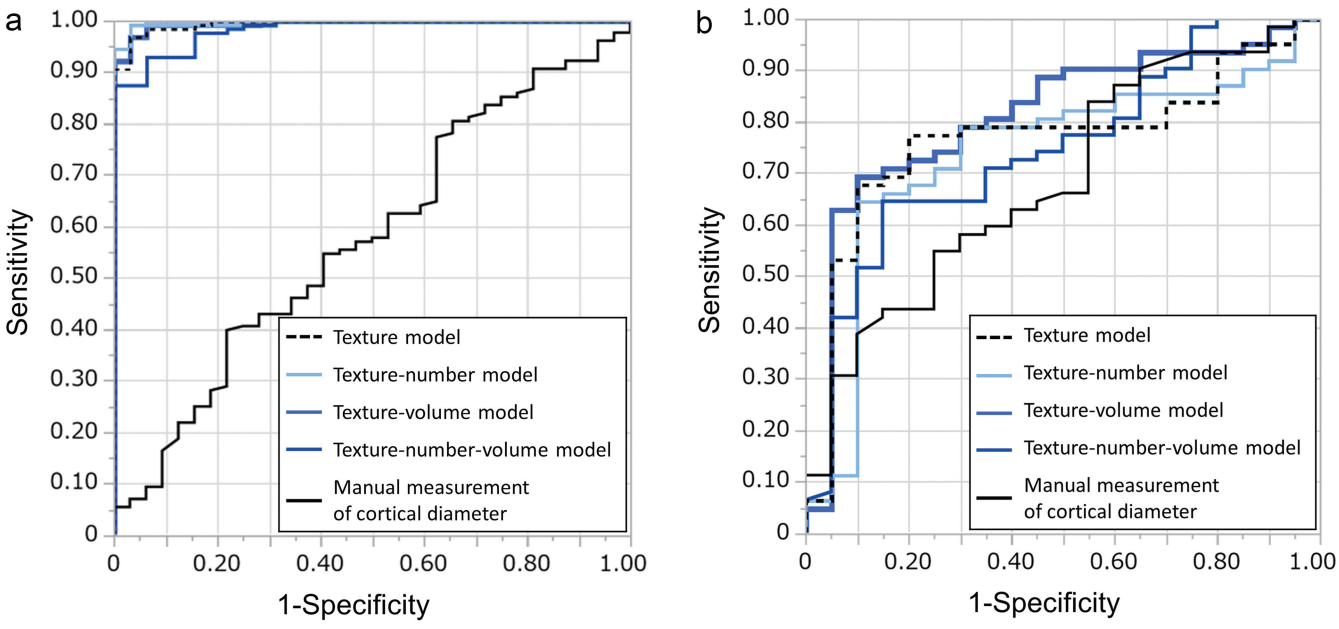

Fig. 3 Graphs depicting the ROC curve analysis using AUCs for the texture model, texture-number model, texture-volume model, texture-number-volume model, and manual measurement of the cortical diameter for differentiating between positive and negative lymph node metastasis in the training (**a**) and validation cohorts (**b**). A comparison of AUCs in the validation cohort demonstrates higher diagnostic performance of the texture-volume model (0.8129) than that of the texture model (0.7677), the texture-number model (0.7403), the texture-number-volume model (0.7448), and the manual measurement of the cortical diameter (0.6851). AUCs, area under the curves; ROC, receiver operating characteristic.

assessment of LN metastasis in patients with breast cancer.[16] Our results focusing on patients with clinically node-negative breast cancer highlighted the utility of high-resolution 3D T2WI with bilateral breast coils in distinguishing positive and negative LN metastasis groups, thereby supporting the findings of Samiei et al.[16] Previous studies used visual heterogeneity of signal intensity on T2WI within LNs as an evaluation criterion for distinguishing positive and negative LN metastasis.[10,19] Texture analysis can capture and quantify patterns of signal intensity on images.[25,26,30,31] In this study, texture analysis of high-resolution 3D T2WI focused on the axillary region and facilitated distinguishing positive and negative LN metastasis groups. The texture analysis may supposedly capture the heterogeneity of signal intensity in the LNs caused by histological changes such as necrosis, angiogenesis, and histiocyte aggregation caused by metastasis.[32–34]

We observed a significant difference in the total volume of all LNs between the positive and negative LN metastasis groups both in the training and validation cohorts. In addition, the texture-volume model displayed a higher diagnostic performance than other texture models combining the number of LNs or the total volume of all LNs, thus indicating the total volume of all LNs had an added value in discriminating between positive and negative LN metastasis. The number of LNs was significantly different between the positive and negative LN metastasis groups in the training cohort, but not in the validation cohort. The diagnostic performance of the model with the number of LNs did not exceed that of the texture-volume model. In mice experimental studies of LN metastasis, the internal pressure increased in distant non-metastatic LNs, other than in metastatic LNs. Furthermore, histological changes occurred in non-metastatic LNs, despite not being accompanied by metastasis.[35,36] Such changes in metastatic and non-metastatic LNs may increase the total volume of all LNs in patients with breast cancer and LN metastasis. This warrants future animal and clinical studies to confirm the mechanism of an increase in the total volume of all LNs.

We calculated the least axis length of LNs by PyRadiomics as the smallest axis length of the ellipsoid enclosing the VOI. It was regarded as a parameter similar to the largest cortical diameter of the LN, and the segmented LNs were ordered from the largest LN to the smallest LN based on the least axis length in each case. To extract reliable texture features from the most suspicious LNs, we selected the LNs with the largest least axis length. One reason was that a large number of voxels as much as possible might be required for the texture analysis. Texture features are calculated by adding the relationship between the signal intensity of neighboring voxels within VOIs,[25] and features from a larger volume are considered more reliable.[37,38] The second reason is that several studies on LN metastasis in breast cancer have demonstrated that an increase in the short axis length of LNs is one of the suggestive findings of metastatic LNs.[10,12,19,39] Therefore, we used the least axis length as the parameter for selecting the most suspicious LNs. All visible LNs were segmented for texture analysis, and the number of LNs varied among cases. Using the mean value of each feature is one method for using the texture features from all LNs for model construction. However, the mean value of each feature might not be appropriate because features from metastatic and non-metastatic LNs were averaged. Indeed, the diagnostic performance of the mean value of texture features was insufficient for distinguishing the positive and negative LN metastasis groups (Appendix).

Baltzer et al. reported an increased number of LNs on the affected side, compared with the contralateral side in patients with breast cancer.[9] In this study, we did not image the contralateral axillary region, thus necessitating future studies with high-resolution 3D T2WI of the bilateral axillary region.

Only few studies have attempted to discriminate positive and negative LN metastasis using MRI in clinically node-negative breast cancer cases.[40] Our texture-volume model could detect LN metastasis in patients with clinically node-negative breast cancer with a sensitivity of 90%, which may enable the prediction of prognosis and the indication of neoadjuvant therapy. The result of 96% NPV indicated that clinicians may avoid unnecessary sentinel LN biopsy using this texture-volume model. We manually segmented all visible LNs in 242 cases. This segmentation process is time-consuming, and the development of automatic segmentation appears essential for the clinical application of texture analysis of high-resolution 3D T2WI in diagnosing LN metastasis.[41,42]

This study had several limitations. First, the sample size of positive LN metastasis cases was small, and there was a significant difference in the age between the training and validation cohorts. This necessitates further study with a larger sample size to confirm our results. Second, we excluded cases with severe noise and artefacts. Focusing on the FOV and increased matrix size to improve the spatial resolution caused the degradation of SNR and aliasing artefacts, thus warranting technical development to improve the image quality of high-resolution 3D T2WI. Third, the generalization ability of high-resolution 3D T2WI has not been confirmed. 3D T2WI provides comparable contrast and improved depiction of lesion morphology in the breast in comparison to 2D T2WI, and it is routinely used in breast MRI protocol.[43] In this study, high-resolution 3D T2WI was imaged at 3T MR system at our institution; however, we do not know whether similar image quality sufficient for texture analysis of LNs can be obtained on 3T or 1.5T MR systems at other institutions. Therefore, a multicenter study on other MRI units at different institutions is required to confirm our results. Fourth, the exclusion of patients who underwent neoadjuvant treatment may have resulted in a selection bias with the tendency toward patients with luminal type or early-stage breast cancer. Furthermore, we did not perform a

subgroup analysis based on histological types, such as invasive lobular carcinoma and mucinous carcinoma. This necessitates a detailed subgroup analysis to construct models based on intrinsic subtypes (luminal, human epidermal growth factor 2 [HER2], and triple negative), stages, and histological types of breast cancer. Fifth, the interobserver reliability of the segmentation of LNs was not confirmed in this study. We used 3D T2WI without fat suppression for imaging axillary LNs. Segmentation of the LNs was not difficult because the LNs, blood vessels, and muscles were visualized as low-signal intensity in the axillary fat (high-signal intensity). It is expected that any observer can easily segment LNs with a high agreement. However, the segmentation of multiple LNs is time-consuming, and it is desirable to develop an automatic segmentation system for LNs in the future.

Conclusion

The texture-volume model combining texture features from the LN with the largest least axis length and the total volume of all LNs on axillary high-resolution 3D T2WI effectively distinguished positive and negative LN metastasis for patients with clinically node-negative breast cancer.

Acknowledgments

The authors thank Taiki Yamamoto, Hiromu Yurimoto, Ken Hasegawa, Koki Yatsuduka, and Sho Nakamura in Tohoku University for their kind support in data collection.

Funding

This study has received funding from JSPS (Japan Society for the Promotion of Science) 21K07559 and 18K07742.

Conflicts of Interest

The authors declare that they have no conflicts of interest.

Appendix

We averaged 90 texture features obtained from all lymph nodes (LNs) in each patient. For the average texture features, we performed feature selection using the least absolute shrinkage and selection operator (LASSO) algorithm to construct an average texture model by Random Forest. We evaluated the diagnostic performance of the average texture model constructed on the training cohort in differentiating between the positive and negative LN metastasis groups using receiver operating characteristic (ROC) curve analysis.

During feature selection using the LASSO algorithm, four features with non-zero coefficients were selected for average texture features: first order skewness, GLCM difference variance, GLCM MCC, gray level run length matrix short run emphasis, gray level size zone matrix large area emphasis. The area under the curves of the average texture model in the training and validation cohorts were 0.8779 and 0.6681, respectively.

Supplementary Information

A supplementary file is available online.

Supplementary Table 1
Ninety texture features for high-resolution 3D T2 weighted images.

References

1. Nemoto T, Vana J, Bedwani RN, Baker HW, McGregor FH, Murphy GP. Management and survival of female breast cancer: Results of a National Survey by the American College of Surgeons. *Cancer* 1980; 45:2917–2924.
2. Banerjee M, George J, Song EY, Roy A, Hryniuk W. Tree-based model for breast cancer prognostication. *J Clin Oncol* 2004; 22:2567–2575.
3. Cianfrocca M, Goldstein LJ. Prognostic and predictive factors in early-stage breast cancer. *Oncologist* 2004; 9:606–616.
4. Beenken SW, Urist MM, Zhang Y, et al. Axillary lymph node status, but not tumor size, predicts locoregional recurrence and overall survival after mastectomy for breast cancer. *Ann Surg* 2003; 237:732–739; discussion 738–739.
5. Goldhirsch A, Winer EP, Coates AS, et al. Personalizing the treatment of women with early breast cancer: highlights of the St Gallen International Expert Consensus on the Primary Therapy of Early Breast Cancer 2013. *Ann Oncol* 2013; 24:2206–2223.
6. Cardoso F, Kyriakides S, Ohno S, et al. Early breast cancer: ESMO Clinical Practice Guidelines for diagnosis, treatment and follow-up. *Ann Oncol* 2019; 30:1194–1220.
7. Kuijs VJL, Moossdorff M, Schipper RJ, et al. The role of MRI in axillary lymph node imaging in breast cancer patients: a systematic review. *Insights Imaging* 2015; 6:203–215.
8. American College of Radiology. Breast Imaging Reporting and Data System (BI-RADS), 5th Ed. 2013.
9. Baltzer PAT, Dietzel M, Burmeister HP, et al. Application of MR mammography beyond local staging: Is there a potential to accurately assess axillary lymph nodes? Evaluation of an extended protocol in an initial prospective study. *AJR Am J Roentgenol* 2011; 196:W641–W647.
10. Luciani A, Dao TH, Lapeyre M, et al. Simultaneous bilateral breast and high-resolution axillary MRI of patients with breast cancer: preliminary results. *AJR Am J Roentgenol* 2004; 182:1059–1067.
11. Kim SH, Shin HJ, Shin KC, et al. Diagnostic performance of fused diffusion-weighted imaging using T1-weighted imaging for axillary nodal staging in patients with early breast cancer. *Clin Breast Cancer* 2017; 17:154–163.
12. Kim EJ, Kim SH, Kang BJ, Choi BG, Song BJ, Choi JJ. Diagnostic value of breast MRI for predicting metastatic axillary lymph nodes in breast cancer patients: diffusion-weighted MRI and conventional MRI. *Magn Reson Imaging* 2014; 32:1230–1236.

13. Fujii T, Yanagita Y, Fujisawa T, Hirakata T, Iijima M, Kuwano H. Implication of extracapsular invasion of sentinel lymph nodes in breast cancer: Prediction of nonsentinel lymph node metastasis. *World J Surg* 2010; 34:544–548.
14. Nottegar A, Veronese N, Senthil M, et al. Extra-nodal extension of sentinel lymph node metastasis is a marker of poor prognosis in breast cancer patients: A systematic review and an exploratory meta-analysis. *Eur J Surg Oncol* 2016; 42:919–925.
15. Schipper RJ, Paiman ML, Beets-Tan RGH, et al. Diagnostic performance of dedicated axillary T2-and diffusion-weighted MR imaging for nodal staging in breast cancer. *Radiology* 2015; 275:345–355.
16. Samiei S, Smidt ML, Vanwetswinkel S, et al. Diagnostic performance of standard breast MRI compared to dedicated axillary MRI for assessment of node-negative and node-positive breast cancer. *Eur Radiol* 2020; 30:4212–4222.
17. Shimizu H, Mori N, Ren H, et al. Multimodal imaging findings including high-resolution 3D T2-weighted imaging for COVID-19 vaccine-associated axillary lymphadenopathy in a patient with breast cancer. *Radiol Case Rep* 2022; 17:2831–2836.
18. Brouwer NPM, Stijns RCH, Lemmens VEPP, et al. Clinical lymph node staging in colorectal cancer; a flip of the coin? *Eur J Surg Oncol* 2018; 44:1241–1246.
19. Atallah D, Moubarak M, Arab W, el Kassis N, Chahine G, Salem C. MRI-based predictive factors of axillary lymph node status in breast cancer. *Breast J* 2020; 26:2177–2182.
20. Haralick RM, Shanmugam K, Dinstein I. Textural features for image classification. *IEEE Trans Syst Man Cybern* 1973; SMC-3:610–621.
21. Song J, Hu Q, Ma Z, Zhao M, Chen T, Shi H. Feasibility of T2WI-MRI-based radiomics nomogram for predicting normal-sized pelvic lymph node metastasis in cervical cancer patients. *Eur Radiol* 2021; 31:6938–6948.
22. Samiei S, Granzier RWY, Ibrahim A, et al. Dedicated axillary MRI-based radiomics analysis for the prediction of axillary lymph node metastasis in breast cancer. 2021
23. Chang JM, Leung JWT, Moy L, Ha SM, Moon WK. Axillary nodal evaluation in breast cancer: State of the art. *Radiology* 2020; 295:500–515.
24. Alhamzawi R, Ali HTM. The Bayesian adaptive lasso regression. *Math Biosci* 2018; 303:75–82.
25. Mori N, Abe H, Mugikura S, et al. Discriminating low-grade ductal carcinoma in situ (DCIS) from non-low-grade DCIS or DCIS upgraded to invasive carcinoma: effective texture features on ultrafast dynamic contrast-enhanced magnetic resonance imaging. *Breast Cancer* 2021; 28:1141–1153.
26. Ren H, Mori N, Mugikura S, et al. Prediction of placenta accreta spectrum using texture analysis on coronal and sagittal T2-weighted imaging. *Abdom Radiol (NY)* 2021; 46:5344–5352.
27. Landis JR, Koch GG. The measurement of observer agreement for categorical data. *Biometrics* 1977; 33:159–174.
28. van Nijnatten TJA, Schipper RJ, Lobbes MBI, et al. Diagnostic performance of gadofosveset-enhanced axillary MRI for nodal (re)staging in breast cancer patients: results of a validation study. *Clin Radiol* 2018; 73:168–175.
29. Mori N, Tsuchiya K, Sheth D, et al. Diagnostic value of electric properties tomography (EPT) for differentiating benign from malignant breast lesions: comparison with standard dynamic contrast-enhanced MRI. *Eur Radiol* 2019; 29:1778–1786.
30. Lafcı O, Celepli P, Seher Öztekin P, Koşar PN. DCE-MRI radiomics analysis in differentiating luminal A and luminal B breast cancer molecular subtypes. *Acad Radiol* 2023; 30:22–29.
31. Kayadibi Y, Kocak B, Ucar N, Akan YN, Yildirim E, Bektas S. MRI radiomics of breast cancer: Machine learning-based prediction of lymphovascular invasion status. *Acad Radiol* 2022; 29(Suppl1):S126–S134.
32. Mori N, Mugikura S, Miyashita M, et al. Perfusion contrast-enhanced ultrasound to predict early lymph-node metastasis in breast cancer. *Jpn J Radiol* 2019; 37:145–153.
33. Lorusso G, Rüegg C. New insights into the mechanisms of organ-specific breast cancer metastasis. *Semin Cancer Biol* 2012; 22:226–233.
34. Garces S, Yin CC, Miranda RN, et al. Clinical, histopathologic, and immunoarchitectural features of dermatopathic lymphadenopathy: an update. *Mod Pathol* 2020; 33:1104–1121.
35. Miura Y, Mikada M, Ouchi T, et al. Early diagnosis of lymph node metastasis: Importance of intranodal pressures. *Cancer Sci* 2016; 107:224–232.
36. Nathanson SD, Mahan M. Sentinel lymph node pressure in breast cancer. *Ann Surg Oncol* 2011; 18:3791–3796.
37. Kölhi P, Järnstedt J, Sikiö M, et al. A texture analysis method for MR images of airway dilator muscles: a feasibility study. *Dentomaxillofac Radiol* 2014; 43:20130403.
38. He Z, Huston DR, Grimm S, et al. Dependence of tissue characterization features on region of interest (ROI) size: studies on phantoms and simulations. Proceedings of IEEE Ultrasonics Symposium, Montreal, 2004; 3:2082–2085.
39. He N, Xie C, Wei W, et al. A new, preoperative, MRI-based scoring system for diagnosing malignant axillary lymph nodes in women evaluated for breast cancer. *Eur J Radiol* 2012; 81:2602–2612.
40. Zhang X, Yang Z, Cui W, et al. Preoperative prediction of axillary sentinel lymph node burden with multiparametric MRI-based radiomics nomogram in early-stage breast cancer. *Eur Radiol* 2021; 31:5924–5939.
41. Zhao X, Xie P, Wang M, et al. Deep learning–based fully automated detection and segmentation of lymph nodes on multiparametric-mri for rectal cancer: A multicentre study. *EBioMedicine* 2020; 56:102780.
42. Liu X, Sun Z, Han C, et al. Development and validation of the 3D U-Net algorithm for segmentation of pelvic lymph nodes on diffusion-weighted images. *BMC Med Imaging* 2021; 21:170.
43. Moran CJ, Hargreaves BA, Saranathan M, et al. 3D T2-weighted spin echo imaging in the breast. *J Magn Reson Imaging* 2014; 39:332–338.